14th International Symposium on Turbulence and Shear Flow Phenomena (TSFP14)
Heidelberg, Germany, July 28-31, 2026

DIRECT NUMERICAL SIMULATION OF A TURBULENT PLANE COUETTE FLOW OVER A ROD-ROUGHENED WALL

Sung Min Lee
Department of Mechanical Engineering
UNIST
50 UNIST-gil, Eonyang-eup, Ulsan, 44919, Korea
lsm9598@unist.ac.kr

Jae Hwa Lee
Department of Mechanical Engineering
UNIST
50 UNIST-gil, Eonyang-eup, Ulsan, 44919, Korea
jhlee06@unist.ac.kr

ABSTRACT

A direct numerical simulation of a turbulent plane Couette flow over a two-dimensional (2D) rod-roughened wall is conducted to examine the effect of surface roughness on this type of flow. The turbulent Couette flow is driven by imposing a constant velocity on the top wall, with transverse 2D rods periodically arranged in the streamwise direction on only the stationary bottom wall. The roughness height (k) and width (w) employed are 0.2h (h is the channel-half height) and the streamwise spacing between the roughness elements (p) is set to p/k =10. A comparison of the root-mean-square of the streamwise velocity fluctuations (u'_{rms}) between smooth- and rough-wall Couette flows (hereafter, SCF and RCF) shows that the turbulence activity in the outer layer for the RCF decreases compared to that of the SCF due to the abatement of the large-scale negative u'-component, indicating that the wall-similarity hypothesis between the SCF and RCF in the outer layer is not established. The weakening of the large-scale negative u'-component in the outer layer results from the reduced streamwise coherence of the large-scale u'-structure in the outer layer with the decreased energy. In addition, linear estimates for conditional structures demonstrate that the reduced coherence of the large-scale u'-structure with less energy in the outer layer for the RCF is found to occur due to the suppressed development of a hairpin packet resulting from the weakened roll-cell motions with less influence on the near-wall region.

INTRODUCTION

The effects of surface roughness on canonical wall-bounded turbulent flows have been extensively studied thus far given the significantly influence of rough surfaces on certain turbulent properties, such as the transport of mass, momentum and heat. Townsend (1976) stated that turbulence outside a roughness sublayer is independent of the surface roughness and that the interaction between the inner and outer layers is weak at a high Reynolds number (hereafter referred to as Townsend's wall-similarity hypothesis). A number of studies have also demonstrated the validity of Townsend's wall-similarity hypothesis in TBLs for irregular and topological three-dimensional (3D) roughness elements.

In addition to previous observations of TBL flows over irregular 3D roughness, many studies of TBL flows over regular two-dimensional (2D) and 3D surface roughness have been conducted experimentally and numerically. Krogstad and Antonia (1999) performed an experiment in a TBL with a circular 2D rod-roughened surface, finding that the surface geometry significantly affects the turbulent energy production and turbulent diffusion in the outer layer, contrary to TBL flows over irregular 3D roughness. In a direct numerical simulation (DNS) study, Lee and Sung (2007) showed that 2D rod roughness (δ/k = 20) can lead to an increase in the Reynolds stresses in the outer layer. Similarly, Lee *et al*. (2011) found that 3D cube roughness affects the turbulence in the outer layer, although the roughness effects of the cube are less significant than those of a 2D rod when the roughness height is identical. Furthermore, Volino *et al*. (2009), by comparing turbulent structures over a smooth wall, reported that an increase in the Reynolds stress in the outer layer can be caused by large-scale turbulent motions originating from the 2D and 3D surface roughness. The results between cube and sinusoidal roughness elements indicate that square-edged roughness induces strong interaction between the inner and outer layers due to blockage effects.

Consistent with the observations in TBLs, previous studies involving fully developed turbulent channel flows (i.e., turbulent Poiseuille flow) with one-sided 2D rod roughness have shown an absence of wall similarity in the outer layer. For one-sided turbulent channel flows over 2D rods with k/h = 0.1 (where h is the channel half-height), Burattini *et al*. (2008) showed that the influence of the roughness extends to beyond the channel centerline by investigating profiles of the Reynolds stresses and skewness. Furthermore, Bhaganagar *et al*. (2004) reported that for egg-carton-shaped roughness arranged on one side of a plane channel wall, the turbulent intensities increase significantly in the outer layer compared to that for a smooth wall channel flow, while the vorticity fluctuations are not affected by the surface roughness.

Aside from canonical TBL flows and Poiseuille flows, turbulent plane Couette flows, derived from the moving velocity on the bottom and/or top wall(s), are frequently observed in many engineering applications. These flows are known to be characterized by the organization of large-scale streaky patterns throughout the entire flow, even at a low Reynolds number, and these streamwise-oriented streaks appear as secondary roll-cell motions with an outer peak in the energy spectra of the velocity fluctuations. Because the surfaces of the turbulent plane Couette flow are not often smooth but usually rough, the research on the impact of the surface roughness on a turbulent Couette flow is a necessary step to gain a better understanding of the turbulent Couette flow in the actual flow environment. However, few studies have sought to investigate the effects of the surface roughness on turbulent plane Couette flows, except for a DNS study by Javanappa and Narasimhamurthy (2021) at a very low Reynolds number (Re_τ = 110) (where Re_τ is the friction Reynolds number). Although they carried out a useful comparison of k-type and d-type 2D rod-roughened turbulent plane Couette flows with a smooth-wall turbulent plane Couette flow, they mostly focused on an analysis of the near-wall influence of the surface roughness.

In the present study, a DNS of the turbulent plane Couette flow with 2D rod roughness at a moderate Reynolds number (Re_τ

≈ 250) is conducted to provide a clear understanding of the influence of the surface roughness in the outer layer, with specific attention paid to the modification of large-scale features. Because the fundamental mechanisms of heat and momentum transfer are largely affected by the dynamics of large-scale structures in the outer region of the wall turbulence, studying the modification of large-scale features by the surface roughness will be able to improve our understanding to the impact of the surface roughness. First, we assess the establishment of the wall-similarity hypothesis in the outer layer in comparison to data for a smooth-wall turbulent plane Couette flow. Subsequently, to explain the possible origin of the lack of outer-layer wall-similarity between the rough and smooth wall flows, the effects of surface roughness on the large-scale structures in the outer layer are identified based on an analysis of spatial features for streamwise velocity-fluctuating structures. The linearly estimated conditional flow field, which is based on two-point correlation coefficients between the vortex strength and velocity fluctuations, shows that the reduced spatial coherence of large-scale structures with less energy in the outer layer of a rough-wall turbulent Couette flow is due to the suppressed development of hairpin vortices to form a packet. Finally, a spectral filtered conditionally averaged flow field with a Q2-event vector is analyzed to discuss why small-scale motions do not form a packet less frequently for a RCF than for a SCF based on modified roll-cell motions.

Numerical Method

For an incompressible flow, the non-dimensional governing equations are

$$\frac{\partial u_i}{\partial t}+\frac{\partial u_i u_j}{\partial x_j}=-\frac{\partial p}{\partial x_i}+\frac{1}{Re_C}\frac{\partial^2 u_i}{\partial x_j \partial x_j}+f_i, \qquad (1)$$

$$\frac{\partial u_i}{\partial x_i}-q=0, \qquad (2)$$

where u_i represents the corresponding velocity components and x_i denotes the Cartesian coordinates in the i-direction (i = 1 ~ 3). The notation adopted here is such that u (= u_1), v (= u_2), and w (= u_3) denote the velocity components of the streamwise, wall-normal, and spanwise directions, respectively, and x (= x_1), y (= x_2), and z (= x_3) denote the corresponding coordinates. All variables are non-dimensionalized by the smooth wall laminar centerline velocity (U_C) and the channel half-height (h), and the Reynolds number is defined as $Re_C = U_C h/\nu$, where ν is the kinematic viscosity. In the present study, the immersed boundary method is used to describe the surface roughness in the Cartesian coordinates with a rectangular domain (Kim *et al*., 2001). The discrete-time momentum forcing f_i is explicitly calculated in time to impose a no-slip condition on the immersed boundary. To satisfy the mass conservation, a mass source/sink term, q, is introduced for the cell containing the immersed boundary.

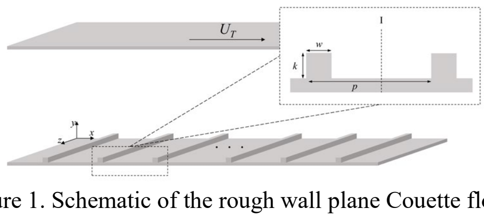

Figure 1. Schematic of the rough wall plane Couette flow.

Figure 1 shows a schematic of the computational domain for the turbulent plane Couette flow with 2D rod roughness. Hereafter, SCF and RCF indicate turbulent plane smooth and rough wall Couette flows, respectively. Transverse 2D rods are periodically arranged in the streamwise direction only on the bottom wall. The streamwise spacing between the roughness elements (p) is selected as p/k =10 and the roughness height (k) and width (w) employed in this study are 0.2h. The center of the roughness valley, location I, is defined for scrutiny of the turbulence statistics in the presence of the rough walls. A no-slip boundary condition (U_B = 0) is adopted on the bottom wall, and the boundary condition for a constant velocity, $U_T = 2U_C$, at the top wall is applied to drive a Couette flow. The subscripts "B" and "T" indicate a bottom wall and a top wall, respectively. Periodic boundary conditions are imposed in the streamwise and spanwise directions. The mean pressure gradient is zero. A non-uniform grid is employed in the wall-normal direction and a uniform grid is adopted in both the streamwise and spanwise directions. To obtain the converged turbulent statistics, phase- (or plane-) and time-averaging techniques are employed for the SCF and RCF. The phase- and temporal-averaged mean quantities are denoted by capital letters or in brackets, e.g., U_i and $<u'v'>$, and the velocity fluctuations (u_i') are defined as $u_i' = u_i - U_i$.

Table 1. Numerical details for DNSs of each case.

Case	Re_C	$Re_{\tau B}$	L_x/h	L_y/h	L_z/h	N_x, N_y, N_z
SCF	4500	243	10π	2	3 π	1025,257,641
RCF	4500	357	10π	2	3 π	1537,257,641

The computational domain size, mesh resolution, and flow parameters are summarized in Table 1. The superscript + indicates statistics normalized by the mean friction velocity ($U_{\tau B}$) on each bottom wall for the SCF and RCF. The mean friction velocity ($U_{\tau B}$) for the RCF is estimated from the total drag defined as the sum of the mean skin frictional and form drags averaged on the horizontal plane (Leonardi *et al*., 2003). Since the bulk Reynolds number is fixed for the SCF and RCF (Re_C = 4500) in the present study, an additional drag component for the RCF (i.e., form drag) caused by a pressure gradient between the upstream and downstream walls of an individual roughness element increases Re_τ for the RCF. However, because the difference in the friction Reynolds number is not large, the effect of the Reynolds number on our results is negligible.

Turbulent Statistics

The profiles of the rms of the streamwise velocity fluctuations (u'^+_{rms}) for the SCF and RCF in the outer coordinates normalized by $U_{\tau B}$ are shown in figure 2(a). Here, u'^+_{rms} for the SCF (black line) shows a near-wall peak at $y/h \approx 0.06$ ($y^+ \approx 15$) due to the near-wall self-sustaining cycle and the peak magnitude of u'^+_{rms} is larger than that for a smooth-wall turbulent Poiseuille flow due to the presence of very long structures (Tsukahara *et al*. 2006). As surface roughness is imposed on the bottom wall, u'^+_{rms} near the bottom wall is reduced (red line) owing to the blockage effect of the rod roughness. Compared to the data for the SCF, u'^+_{rms} in the outer layer for the RCF decreases, indicating that the wall-similarity hypothesis in the outer layer is not established for the RCF. However, this behavior is obviously contrary to earlier findings showing that the streamwise Reynolds stress in the outer layer increases in TBL flows (Lee and Sung, 2007) and in a turbulent Poiseuille flow (Nagano *et al*., 2004) with 2D rod roughness. To identify the contribution of the scale of the turbulent motion to the reduction of u'^+_{rms} in the outer layer, the decomposition of u'^+_{rms} into large- and small-scale components based on a cutoff wavelength of λ_z/h = 1.0, where λ_z is the spanwise wavelength, is conducted, as shown in figure 2(b). The decomposition shows that the introduction of surface roughness leads to a significant decrease of the large-scale component in the outer layer while the modification of the small-scale component is negligible. Thus, the analysis of the scale-decomposed u'^+_{rms} reveals that the reduction of the turbulent activities for the RCF is mostly attributed to the weakening of the large-scale u'-structure in the outer layer.

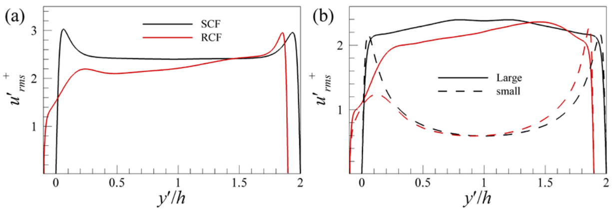

Figure 2. (a) Profiles of the root-mean-square of the streamwise velocity fluctuations and (b) their decomposition into large- (solid line) and small-scale (dashed line) components.

Spatial Organization of Streamwise Velocity-Fluctuating Structures

To provide statistical evidence of the modified spatial organization patterns of the large-scale u'-structures by the imposition of surface roughness, the two-point spatial correlation coefficients of the streamwise velocity fluctuations with an increase in the reference height (y_r) are investigated for the SCF and RCF. Here, to identify the individual effects of the surface roughness on the large-scale turbulent structures, we consider the large-scale (u_l') components, which are shown in figures 8. The two-point correlation coefficients for the large- and small-scale components are defined as follows:

$$R_{u_l' u_l'}(r_x, r_y = 0, r_z; x_r, y_r) = \frac{\langle u_l'(x_r, y_r, z_r) u_l'(x_r + r_x, y_r + r_y, z_r + r_z) \rangle}{\sigma_{u'}^2} \quad (3)$$

where the spatial shifts from the reference positions x_r, y_r and z_r are represented as r_x, r_y and r_z, with $\sigma_{u'}$ as the rms of u'. For a horizontal plane, r_y = 0, and the correlation coefficient is independent of the reference position of z_r due to the homogeneity of the flow in the spanwise direction. The large-scale components of u_l' are extracted based on the cutoff wavelength λ_z/h = 1.0.

For the SCF in figure 3(a), the general appearance of a correlation with a streamwise elongated positive-correlation region (red contour) flanked by negative-correlation regions (blue contour) in the spanwise direction at y_r'/h = 0.2, 0.5 and 1.0 is similar to that in a previous study of a turbulent Couette flow over a smooth wall with a very long domain. The streamwise length scale for the large-scale structures increases continuously in the outer layer. When surface roughness is introduced on the bottom wall, as shown in figure 3(b), the alternating low- and high-correlation patterns are similar to those for the SCF. However, the streamwise coherence is reduced by 4~50% compared to that for the SCF along y_r'/h, although the increasing trend of the streamwise length scale for the large-scale structure is similar to that for the SCF. Contrary to the reduction of the streamwise length scale, the spanwise length scale of the large-scale structures in the outer layer for the RCF is approximately 5% larger than that for the SCF due to the influence of the infinite spanwise length scale of the rod roughness, similar to a previous observation for a TBL flow over rod roughness by Lee *et al*. (2016).

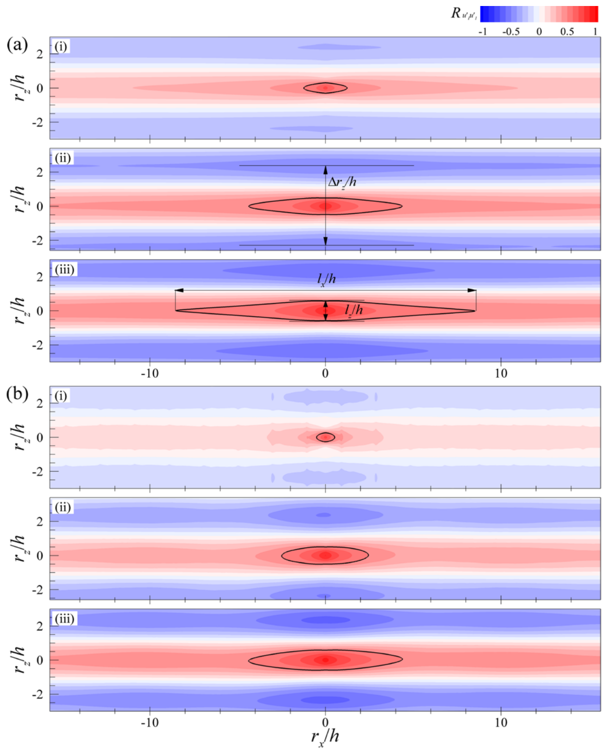

Figure 3. Contours of the spatial two-point correlation coefficients of the large-scale streamwise velocity-fluctuation on the r_x-r_z plane for the (a) SCF and (b) RCF: (i) y_r'/h = 0.2, (ii) y_r'/h = 0.5 and (iii) y_r'/h = 1.0.

The spanwise wavelength ($\Delta r_z/h$) of the positive- and negative-correlation patterns for the SCF and RCFis estimated to be approximately 4.7 throughout all reference heights, suggesting the superposition of large-scale turbulent structures near the channel centerline on the entire channel. Because it is reported that the large-scale structures with long spatial coherence in the outer layer contribute largely to the generation of the turbulent energy and play a crucial role in generating and transporting turbulent kinetic energy and Reynolds shear stress, the present findings suggest that the weakening of the large-scale negative u'-component in the outer layer is due to the reduced streamwise coherence of the large-scale u'-structure in the outer layer caused by the imposition of surface roughness.

Spanwise Energy Spectra

Not only to examine the modification of the energy distributions by the imposition of surface roughness but also to identify the dominant contribution of the wavelengths to the reduction of u'^+_{rms}, the pre-multiplied spanwise energy spectra of the streamwise velocity fluctuations are plotted in figure 4. The definition of the spectrum, $\Phi_{u'u'}$, with spatial homogeneity in the spanwise direction is as follows: $\Phi_{u'u'}(k_z; x_r, y_r) = S_{u'u'}(k_z; x_r, y_r)$ +

$S_{u'u'}(-k_z;\, x_r,\, y_r) = 2Re\{S_{u'u'}(k_z;\, x_r,\, y_r)\}$. Here, $S_{u'u'}$ is the one-dimensional Fourier transform of the correlation coefficient in the spanwise direction:

$$S_{u'u'}(k_z; x_r, y_r) = \frac{1}{2\pi}\int_{-\infty}^{\infty} e^{-jk_z r_z}\left\langle u'(x_r, y_r, z_r)u'(x_r, y_r, z_r + r_z)\right\rangle dr_z \qquad (4)$$

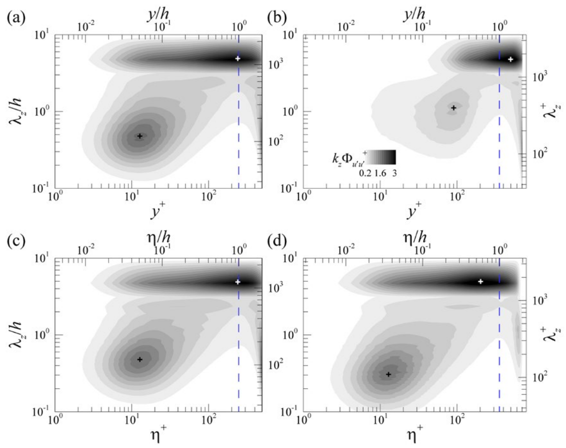

Figure 4. Pre-multiplied spanwise energy spectra of streamwise velocity fluctuations normalized by $U_{\tau B}$: (a) SCF and (b) RCF on the bottom wall and (c) SCF and (d) RCF on the top wall. Vertical blue dashed lines indicate the channel centerline.

For the SCF in figure 4(a), an 'inner peak' is observed at $y^+ = 15$ with $\lambda_z^+ \approx 100$ (black cross symbol), a typical signature of the near-wall cycle of self-sustained quasi-streamwise vortices. At the channel centerline, a 'secondary outer peak' emerges with $\lambda_z/h = 4.7$ (white cross symbol), consistent with the peak-to-peak spanwise wavelength from the contours of the two-point correlation coefficients in figure 3. Because the large-scale energy near the centerline has a footprint on the near-wall region, the outer layer large-scale energy near the centerline is transferred to the near-wall region at the large spanwise wavelength. It should be noted that in a turbulent Couette-Poiseuille flow over a smooth wall, Kim *et al.* (2020) reported that the large-scale structures found in the flow stem from the linear growth of a small-scale structure from each wall to the opposite wall by continuous positive mean shear throughout the entire channel, with the linearly grown large-scale structures between the two walls influencing the entire flow with the generation of a secondary outer peak near the centerline. The features of the contour of the spanwise energy spectrum for the SCF overall are similar to those in Pirozzoli *et al.* (2014) for a smooth-wall plane turbulent Couette flow. As surface roughness is introduced to the turbulent plane Couette flow in figure 4(b), the inner peak shifts to $y^+ \approx 90$ ($y'^+ \approx 55$) with $\lambda_z^+ \approx 400$ and the spectral energy of the peak decreases compared to that for the SCF, similar to a previous observation of a TBL flow over a 2D rod. The location of the secondary outer peak for the RCF is also shifted to a higher wall-normal position ($y'/h = 1.3$ or $y/h = 1.4$), while the peak wavelength is similar to that for the SCF.

Conditional Averaged Flow Fields

In this section, we assess the potential cause of large-scale negative u'-structures with less spatial coherence and energy due to 2D rod roughness. Figure 13 shows the contours of the two-point correlation coefficients between the swirling strength (λ_{ci}) and velocity fluctuations along the streamwise and wall-normal plane ($r_z = 0$) with $y_r'/h = 0.5$. Here, the swirling strength λ_{ci} is calculated from the 2D velocity gradient tensor on the x-y plane to detect only spanwise swirling motion at a reference location.

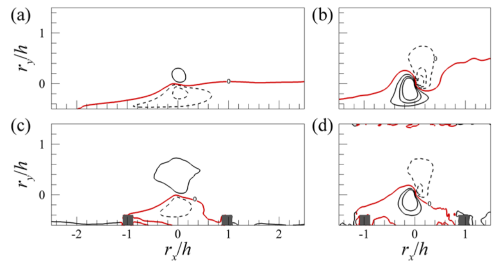

Figure 5. Contours of the two-point correlation coefficients (a, c) between the swirling strength and the streamwise velocity fluctuations ($R_{\lambda u'}$) and (b, d) between the swirling strength and the wall-normal velocity fluctuations ($R_{\lambda v'}$) at $y_r'/h = 0.5$ on the r_x-r_y plane: (a, b) SCF and (c, d) RCF.

For the SCF in figures 5(a) and (b), $R_{\lambda u'}$ is negative below the reference position ($r_x/h = 0$ and $r_y/h = 0$) and positive above the reference position, while $R_{\lambda v'}$ is positive to the left of $r_x/h = 0$ and negative to the right of $r_x/h = 0$. Both contours of $R_{\lambda u'}$ and $R_{\lambda v'}$ reveal the presence of a large-scale inclined interface due to aligned hairpin heads along an inclined line away from the wall. Moreover, a relatively uniform low-speed fluid region is observed under the interface (figure 5a), created by the mutual induction of hairpin vortex heads. The spatial patterns of the streamwise ($R_{\lambda u'}$) and wall-normal ($R_{\lambda v'}$) correlation coefficients for the SCF are in good agreement qualitatively with those in a smooth-wall turbulent channel flow by Christensen and Adrian (2001). When surface roughness is imposed on the bottom wall, the streamwise extents of the negative $R_{\lambda u'}$ (figure 5c) and the positive $R_{\lambda v'}$ (figure 5d) region below the interface are significantly suppressed both downstream and upstream of the reference (or event) location. This result stands in contrast to a previous observation of a large-scale inclined interface that still developed with an increased inclination angle for a TBL flow with 2D rod roughness (Lee *et al*., 2011).

The conditionally averaged velocity vector fields with a λ_{ci} event for the SCF and RCF are illustrated in figure 6 to identify the vortex organization of a packet statistically. The linear stochastic estimation (LSE) of the conditional average based on the conditional event of a positive swirling strength λ_{ci} is given by Christensen and Adrian (2001):

$$\left\langle u_i'(r_x, r_y, r_z) \middle| \lambda_{ci}(x_r, y_r, z_r)\right\rangle = L_i \lambda_{ci}(x_r, r_y, z_r) \qquad (5)$$

with $i = 1$, 2 and 3, and

$$L_i = \frac{\left\langle \lambda_{ci}(x_r, y_r, z_r) u_i'(x_r + r_x, y_r + r_y, z_r + r_z)\right\rangle}{\left\langle \lambda_{ci}(x_r, y_r, z_r)^2\right\rangle} \qquad (6)$$

In the present study, λ_{ci} is given by the rms of λ_{ci} at the reference location (y_r), and the velocity vector in the figure is set to the unit vector to obscure weaker motions away from the event location.

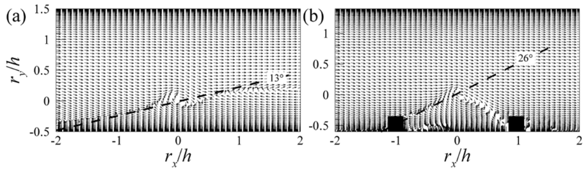

Figure 6. Linear estimates of conditional velocity fields based on a spanwise swirl at y_r'/h = 0.5: (a) SCF and (b) RCF.

In figure 6(a) for the SCF, it is clear that upward motion of a low-speed fluid exists below an inclined large-scale interface, while downward motion of a high-speed fluid is observed above the interface. The mean angle of the inclined interface (dashed line) is approximately 13º, consistent with a previous study by Adrian *et al*. (2000) in which the large-scale structures of hairpin packets were found to grow upward at a mean angle of approximately 12º as they move downstream in a smooth wall TBL flow. Because the flow induced from individual vortex aligns coherently with the flows from successive vortices in a packet, a long region of low-speed fluid is created. When the surface roughness is imposed in figure 6(b), it is clear that behind the vortex core at the event location, the streamwise coherence between the spanwise-oriented vortical structures is totally inhibited with a larger inclination angle (~26°). As a result, a large-scale shear layer of the vortices is not created for the RCF compared to that for the SCF in figure 6(a), indicating that hairpin vortices within the RCF do not form a vortex organization pattern for a hairpin packet coherently in the outer layer and that the backward-induced flows from hairpins do not combine to produce large-scale low-speed fluid in the streamwise direction statistically. Although the inclination angle for the RCF is similar to that for the TBL flow over a rod-roughened wall (~27°), the modification of the vortical structures is obviously distinguishable with regard to previous observations by Lee *et al*. (2011), where a large-scale inclined interface developed for a TBL flow with 2D rod roughness.

The suppressed development of the large-scale features found in figures 5 and 6 clearly contrasts with the current findings through the instantaneous and statistical analyses in figure 3, where long structures are found for the RCF. Thus, it is reasonable to speculate that the suppression of the development of a hairpin packet by the surface roughness found in figures 5 and 6 for the RCF is a statistically masked feature caused by the strong dominance of the small-scale features. In other words, because the numbers of large-scale and small-scale motions are relatively small and large for the RCF compared to the SCF, the LSE can result in the hairpin vortex packet not forming in a statistical sense. Instead, it is correct that the population of the large-scale structures for the RCF decreases compared to that for the SCF.

Roll-Cell Motions

In the previous section, we showed that the reduced streamwise coherence of the large-scale u'-structure with less energy in the outer layer is a direct consequence of the suppression of the development of a hairpin packet caused by surface roughness. Because roll-cell motions in the outer layer have been reported to sweep the small-scale motions beneath them and given that the small-scale motions can ultimately grow into large-scale packet motions via an auto-generation process in canonical wall-bounded turbulent flows, a close examination of the modification of the roll-cell motions caused by the surface roughness could shed light on why the small-scale motions form a packet less frequently in the RCF case. As reported in previous studies by Pirozzoli *et al.* [27], roll-cell motions are typical flow patterns in a SCF, and these motions are closely associated with streamwise-elongated large-scale u'-structures. Thus, a LSE conditioned by a large-scale Q2 event at y_r'/h = 0.5 for the SCF and RCF is performed on the r_y-r_z plane to identify the roll-cell patterns (figure 7). Here, the two-point spatial correlations for the LSE are obtained using the spectral-filtered large-scale velocity fluctuations with a spanwise wavelength of λ_z/h = 1.0 to remove the small-scale features in the turbulent structures. The Q2 event is chosen to maximize the weighted joint probability density function of the large-scale streamwise and wall-normal fluctuations, making the largest contribution to the large-scale second-quadrant Reynolds shear stress.

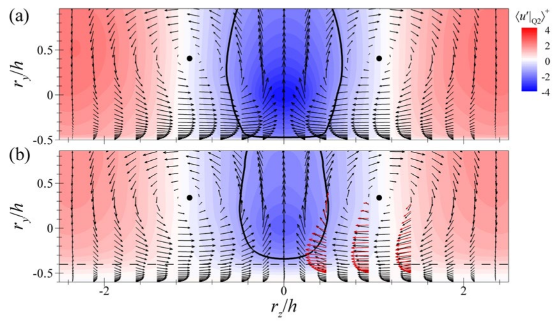

Figure 7. Linear estimates of the large-scale conditional structures based on a Q2-event vector at y_r'/h = 0.5 for the (a) SCF and (b) RCF. The horizontal dashed line in (b) indicates the height of the roughness crest.

The conditional velocity vectors for the SCF in figure 7(a) reveal that the large-scale Q2-event motions are associated with large-scale counter-rotating roll-cell motions with centered low-speed regions, as observed in previous studies of canonical turbulent wall-bounded flows, e.g., Poiseuille flows, TBL flows, Couette flows and Couette-Poiseuille flows. The centered low-speed fluid (shown in blue) for the SCF extends to the near-wall region (see the solid line), indicating the footprint of the large-scale structures onto the near-wall region, consistent with our observation from the energy spectrum in figure 4(a).

However, as surface roughness is introduced to the turbulent plane Couette flow, this footprint of the low-speed regions onto the near-wall region is diminished, as shown in figure 7(b), and a centered low-speed fluid is found above the roughness crest (see the solid line near the bottom wall), indicating that the collective spanwise motion of small-scale motions by the roll cell is intense above the roughness crest (see the horizontal dashed line). In addition, a comparison of the velocity vectors beneath the roll-cell core (see the superimposed velocity vectors shown in red in figure 7b) shows that the strength of the roll-cell motions for the RCF is reduced by the surface roughness with the significant spanwise momentum deficit. It should also be noted that the core locations and sizes of the roll-cell motions are not influenced by the surface roughness, as indicated by the black circles. Because the roll-cell motions centered in the outer layer can sweep the near-wall smaller scales of motions to organize beneath them, the weakened roll cell with active collective spanwise motions above the roughness crest for the

RCF can make the growth of large-scale low-speed structures beneath the roll-cell patterns less frequent compared to the SCF.

Summary and Conclusion

In the present study, we undertook a DNS of a turbulent plane Couette flow with 2D rod roughness to investigate the influence of surface roughness on the structural modification of the large-scale features in the outer layer. The failure of the wall-similarity hypothesis in the outer layer was noted given the reduction of $u'_{rms}{}^{+}$ in the outer layer for the RCF compared to that for the SCF. The spectral decomposition of $u'_{rms}{}^{+}$ into large- and small-scale components showed that the reduction of $u'_{rms}{}^{+}$ for the RCF is attributable to the weakening of the large-scale negative u'-component in the outer layer caused by the imposition of surface roughness. An investigation of the two-point spatial correlations of large-scale streamwise velocity fluctuating structures showed that the streamwise coherence of the large-scale negative u'-structure in the outer layer is reduced by the presence of surface roughness, although the spanwise length scale of the large-scale structures in the outer layer for the RCF is larger than that for the SCF due to the influence of the infinite spanwise length scale of the rod roughness An examination of the spanwise energy spectra of the streamwise velocity fluctuations showed that the inner peak for the RCF occurs at a higher wall-normal location with a larger spanwise wavelength than that for the SCF and that the strength of that peak is weaker compared to that of the SCF. The location of a secondary outer peak for the RCF was also shifted to a higher wall-normal location, while the peak wavelength for the RCF was similar to that for the SCF. Although the peak magnitudes of the large-scale energy were similar between the SCF and RCF, the large-scale energy imprint onto the bottom wall found in the SCF was absent for the RCF, suggesting that the growth and energy transfer process of the large-scale structures on the bottom wall is suppressed by the surface roughness. In order to address the question of why the spatial coherence of the large-scale negative u'-structures is suppressed by the surface roughness, the conditional averaged flow fields were analyzed in detail. Conditional structures with a λ_{ci} event showed that the hairpin vortices for the RCF form a vortex organization pattern for a hairpin packet less frequently in the outer layer than that for the SCF. The suppressed development of the hairpin packet by surface roughness was closely associated with large-scale counter-rotating roll-cell motions, as identified by the large-scale Q2 event. Because the large-scale roll-cell motions centered in the outer layer collect small-scale motions to organize beneath them, the weakened roll-cell motions with less influence on the near-wall region for the RCF led to the generation of large-scale low-speed turbulence motions beneath them less frequently. As a result, fewer large-scale structures were formed for the RCF compared to the SCF, thereby decreasing the turbulent activity in the outer layer for the RCF.

REFERENCES

Townsend AA. 1976. “The Structure of Turbulent Shear Flow”. Cambridge, UK: Cambridge Univ. Press

Krogstad, P. Å., and Antonia, R. A., 1999, "Surface Roughness Effects in Turbulent Boundary Layers," *Experiments in Fluids*, Vol. 27, No. 5, pp. 450-460.

Lee, S. H., and Sung, H. J., 2007, "Direct Numerical Simulation of the Turbulent Boundary Layer Over a Rod-Roughened Wall," *Journal of Fluid Mechanics*, Vol. 584, pp. 125-146.

Lee, J. H., Sung, H. J., and Krogstad, P. Å., 2011, "Direct Numerical Simulation of the Turbulent Boundary Layer Over a Cube-Roughened Wall," *Journal of Fluid Mechanics*, Vol. 669, pp. 397-431.

Volino, R. J., Schultz, M. P., and Flack, K. A., 2009, "Turbulence Structure in a Boundary Layer with Two-Dimensional Roughness," *Journal of Fluid Mechanics*, Vol. 635, pp. 75-101.

Burattini, P., Leonardi, S., Orlandi, P., and Antonia, R. A., 2008, "Comparison Between Experiments and Direct Numerical Simulations in a Channel Flow with Roughness on One Wall," *Journal of Fluid Mechanics*, Vol. 600, pp. 403-426.

Bhaganagar, K., Kim, J., and Coleman, G., 2004, "Effect of Roughness on Wall-Bounded Turbulence," *Flow, Turbulence and Combustion*, Vol. 72, No. 2, pp. 463-492.

Javanappa, S. K., and Narasimhamurthy, V. D., 2021, "Turbulent Plane Couette Flow with a Roughened Wall," *Physical Review Fluids*, Vol. 6, No. 10, p. 104609.

Kim, J., Kim, D., and Choi, H., 2001, "An Immersed-Boundary Finite-Volume Method for Simulations of Flow in Complex Geometries," *Journal of Computational Physics*, Vol. 171, No. 1, pp. 132-150.

Leonardi, S., Orlandi, P., Smalley, R. J., Djenidi, L., and Antonia, R. A., 2003, "Direct Numerical Simulations of Turbulent Channel Flow with Transverse Square Bars on One Wall," *Journal of Fluid Mechanics*, Vol. 491, pp. 229-238.

Tsukahara, T., Kawamura, H., and Shingai, K., 2006, "DNS of Turbulent Couette Flow with Emphasis on the Large-Scale Structure in the Core Region," *Journal of Turbulence*, No. 7, p. N19.

Nagano, Y., Hattori, H., and Houra, T., 2004, "DNS of Velocity and Thermal Fields in Turbulent Channel Flow with Transverse-Rib Roughness," *International Journal of Heat and Fluid Flow*, Vol. 25, No. 3, pp. 393-403.

Lee, J., Kim, J. H., and Lee, J. H., 2016, "Scale Growth of Structures in the Turbulent Boundary Layer with a Rod-Roughened Wall," *Physics of Fluids*, Vol. 28, No. 1.

Kim, J. H., Hwang, J. H., Lee, Y. M., and Lee, J. H., 2020, "Direct Numerical Simulation of a Turbulent Couette-Poiseuille Flow, Part 2: Large- and Very-Large-Scale Motions," *International Journal of Heat and Fluid Flow*, Vol. 86, p. 108687.

Pirozzoli, S., Bernardini, M., and Orlandi, P., 2014, "Turbulence Statistics in Couette Flow at High Reynolds Number," *Journal of Fluid Mechanics*, Vol. 758, pp. 327-343.

Christensen, K. T., and Adrian, R. J., 2001, "Statistical Evidence of Hairpin Vortex Packets in Wall Turbulence," *Journal of Fluid Mechanics*, Vol. 431, pp. 433-443.

Adrian, R. J., Meinhart, C. D., and Tomkins, C. D., 2000, "Vortex Organization in the Outer Region of the Turbulent Boundary Layer," *Journal of Fluid Mechanics*, Vol. 422, pp. 1-54.